Environ Sci Pollut Res (2017) 24:12195–12211
DOI 10.1007/s11356-017-8873-0

RESEARCH ARTICLE

Effect of humic acid preloading on phosphate adsorption onto zirconium-modified zeolite

Jianwei Lin[1] · **Zhe Zhang**[1] · **Yanhui Zhan**[1]

Received: 30 August 2016 / Accepted: 20 March 2017 / Published online: 28 March 2017

Abstract A zirconium-modified zeolite (ZrMZ) was prepared, and then, humic acid (HA) was immobilized on the ZrMZ surface to prepare HA-loaded ZrMZ (HA-ZrMZ). The obtained ZrMZ and HA-ZrMZ were characterized by energy dispersive X-ray spectroscopy, elemental analyzer, N_2 adsorption/desorption isotherms, pH at the point of zero charge, and X-ray photoelectron spectroscopy. The adsorption characteristics of phosphate on ZrMZ and HA-ZrMZ were comparatively investigated in batch mode. The adsorption mechanism of phosphate on ZrMZ and HA-ZrMZ was investigated by ionic strength effect and ^{31}P nuclear magnetic resonance. The mechanism for phosphate adsorption onto ZrMZ was the formation of inner-sphere phosphate complexes at the solid/solution interface. The preloading of HA on ZrMZ reduced the phosphate adsorption capacity, and the more the HA loading amount, the lower the phosphate adsorption capacity. However, the preloading of HA on ZrMZ did not change the phosphate adsorption mechanism; i.e., the formation of inner-sphere phosphate surface complexes was still responsible for the adsorption of phosphate on HA-ZrMZ. The decreased phosphate adsorption capacity for ZrMZ after HA coating could be attributed to the fact that the coating of HA on ZrMZ reduced the amount of binding active sites available for phosphate adsorption, changed the adsorbent surface charges, and reduced the specific surface areas and pore volumes of ZrMZ.

Responsible editor: Philippe Garrigues

✉ Jianwei Lin
jwlin@shou.edu.cn

[1] College of Marine Science, Shanghai Ocean University, No. 999 Hucheng Huan Road, Shanghai 201306, China

Keywords Zirconium-modified zeolite · Humic acid · Preloading · Adsorption · Phosphate

Introduction

Eutrophication has become one of the most severe threats to the health of aquatic ecosystems in freshwater bodies such as rivers, lakes, and reservoirs all over the world, especially in developing countries (Lürling et al. 2014; Smith et al. 1999; Zhang et al. 2015; Zhu et al. 2013). Phosphorus (P) is a vital element to freshwater aquatic ecosystems, and excessive P concentration of overlying waters can cause eutrophication of freshwater bodies (Correll 1998; Smith et al. 1999). Therefore, in order to combat eutrophication of freshwater bodies, it is of great importance to reduce the concentration of P in overlying waters.

The main sources of P in overlying waters include external loading and internal loading. In order to restore the eutrophic freshwater bodies, it is essential for the reduction of the external P loading (Reitzel et al. 2003). However, after a reduction in P external loading, the restoration of eutrophic freshwater bodies is usually delayed by the internal P loading, i.e., the release of P from sediments into overlying waters (Jeppesen et al. 2005; Søndergaard et al. 2003). Therefore, in order to control eutrophication, it is recommended to apply in situ P control technique besides reducing P external loading (Funes et al. 2016).

In situ P control requires both removal of P from overlying water and control of P release from sediment (Lürling et al. 2014). Recently, several solid phase P-sorbents have been proposed for in situ P control, including lanthanum-modified bentonite clay (Lürling et al. 2014; Liu et al. 2016b; Reitzel et al. 2013), aluminum/ferrum-based drinking water treatment residuals (WTRs) (Wang and Pei 2013), natural calcium-rich

sepiolite (NCSP) (Yin et al. 2013), Z2G1-modified zeolite (Gibbs and Özkundakci 2011), calcite (Berg et al. 2004), calcite/zeolite mixture (Lin et al. 2011b), magnetic microparticles (Funes et al. 2016), water clarifier sludge (Ichihara and Nishio 2013), lanthanum-modified soils (Dai and Pan 2014), cationic surfactant-modified sediments (Song et al. 2014), granulated coal ash (Yamamoto et al. 2013), and zirconium-modified zeolite (ZrMZ) (Yang et al. 2014, 2015). Among these P-sorbents, ZrMZ could be an attractive P-sorbent choice for in situ P control because zirconium oxides in ZrMZ had good chemical stability, low solubility in water, and no toxicity, and ZrMZ exhibited a high adsorption capacity for phosphate ions in water and sediment-water systems (Cui et al. 2012; Liu et al. 2008; Rodrigues et al. 2012; Su et al. 2013; Yang et al. 2015).

Humic acid (HA), as an important natural organic matter (NOM), is formed by the microbial breakdown of plant and animal residues and has been found to be widely distributed in natural aquatic systems (Erhayem and Sohn 2014; Wang et al. 2015b). HA contains several functional groups such as carboxyl, phenol, and amine groups (Kumar et al. 2011). HA is known to interact with several metal oxides such as titanium dioxide (Chen et al. 2012), iron oxide (Chekli et al. 2013; Wang et al. 2015b; Yan et al. 2016; Zhou et al. 2014), alumina (Kumar et al. 2011), and silicon dioxide (Liang et al. 2011). HA is also known to interact with zirconium (Stern et al. 2014). When ZrMZ is applied to natural aquatic systems for in situ P control, it may interact with abundant HA. The ZrMZ-HA interaction may alter the surface properties of ZrMZ, and these changes may affect the adsorption behavior of phosphate on ZrMZ. However, there are few studies on the effect of HA coating on the adsorption of phosphate on ZrMZ.

The objective of this study was to determine the effect of HA coating on the adsorption of phosphate from water on ZrMZ. To achieve this goal, two HA-coated ZrMZ (HA-ZrMZ) samples with different HA loading amounts were first prepared. Then, the original ZrMZ and synthesized HA-ZrMZ were comparatively characterized by energy dispersive X-ray spectroscopy (EDX), elemental analyzer, N_2 adsorption/desorption isotherms, pH at the point of zero charge (pH_{PZC}), and X-ray photoelectron spectroscopy (XPS) to explore the influence of HA coating on the surface area, porosity, surface chemical composition and state, etc. Finally, in order to find out the effect of HA coating on adsorption of phosphate onto ZrMZ, the adsorption characteristics and mechanism of phosphate on ZrMZ and HA-ZrMZ were comparatively investigated using batch experiments and solid-state ^{31}P nuclear magnetic resonance (NMR) spectroscopy. Results of this work will be helpful for the application of ZrMZ to remove P from overlying water and to prevent P release from sediments.

Materials and methods

Materials

The original zeolite employed in this work, whose diameter is less than 0.075 mm, was provided from a company in Jinyun County, Zhejiang Province, China. Humic acid was obtained from Aldrich Chemical Company, USA, and used as received. Analytical-grade chemicals used for this study including $ZrOCl_2{\cdot}8H_2O$, KH_2PO_4, NaOH, HCl, NaCl, KCl, $CaCl_2$, $MgCl_2$, $NaHCO_3$, Na_2SO_4, and Na_2SiO_3 were obtained from Sinopharm Chemical Reagent Co., Ltd., China, and used without further purification. Deionized water was chosen to prepare all solutions. The ZrMZ sample was fabricated according to the method reported in our previous study (Yang et al. 2014). The working phosphate solutions with desired concentration were prepared by diluting KH_2PO_4 stock solution to appropriate volumes with deionized water, and their concentrations were all expressed in P.

Preparation of HA-ZrMZ

Two HA-ZrMZ samples were prepared in this study. The HA-ZrMZ sample with relatively low loading amount of HA was prepared as follows. First, 5 g of ZrMZ was mixed with 1 L of HA solution with an initial concentration of 100 mg/L (pH 7) in a 2-L conical flask, and then, the suspension was stirred at 25 °C for 48 h. After that, the suspension was centrifuged at 4000 rpm and the supernatant was poured out. The residue was then washed with deionized water many times to remove freely dissolved HA. Finally, the obtained HA-ZrMZ was air-dried and stored in a closed bottle for further use. Hereafter, the obtained HA-ZrMZ with relatively low loading amount of HA was named as HA-ZrMZ-1.

The ZrMZ sample with relatively high loading amount of HA was prepared as follows. First, the HA-ZrMZ-1 sample was prepared by shaking 5 g of ZrMZ in 1 L of HA solution as described above. Then, the HA-ZrMZ-1 was mixed with 1 L of HA solution with an initial concentration of 100 mg/L (pH 7) in a 2-L conical flask. After that, the suspension was stirred at 25 °C for 48 h. Then, the residue was obtained by centrifugation and washed with deionized water many times to remove freely dissolved HA. Finally, the obtained HA-ZrMZ was air-dried and stored in a closed bottle for further use. Hereafter, the obtained HA-ZrMZ with relatively high loading amount of HA was named as HA-ZrMZ-2.

Characterization of adsorbent materials

An INCA X-Act EDX analyzer (Oxford Instruments, UK) was used to determine the chemical local compositions on the surfaces of ZrMZ, HA-ZrMZ-1, and HA-ZrMZ-2. The

contents of C and N in HA, ZrMZ, HA-ZrMZ-1, and HA-ZrMZ-2 were measured using a Vario EL cube elemental analyzer (Elementar, Germany). The N_2 adsorption/desorption isotherms of the original zeolite, ZrMZ, HA-rMZ-1, and HA-ZrMZ-2 at 77 K were gotten using an ASAP 2020 surface area and porosity analyzer (Micromeritics, USA). Based on the N_2 adsorption isotherm data, the Brunauer-Emmett-Teller (BET) specific surface areas, total pore volumes, and Barret-Joyner-Halenda (BJH) pore diameter distributions of the original zeolite, ZrMZ, HA-ZrMZ-1, and HA-ZrMZ-2 were calculated. The pH_{PZC} values for ZrMZ, HA-ZrMZ-1, and HA-ZrMZ-2 were determined through the pH drift method (Guaya et al. 2015). Brief, an exact 25 mg of adsorbent (ZrMZ, HA-ZrMZ-1, or HA-ZrMZ-2) was added into 20 mL of 0.01 mol/L $NaNO_3$ solutions with initial pH (pH_i) values ranging from 3 to 11, and then, the suspension was shaken for 72 h at 25 °C under interrupted oscillation condition. The final pH (pH_f) value of solution was determined using a pH meter, and the pH_{PZC} value of adsorbent was determined as the pH value at which the addition of adsorbent did not result in a change in the pH value of solution, i.e., $pH_f - pH_i = 0$. A Kratos Axis Ultra^{DLD} spectrometer (Kratos Analytical-A Shimadzu group company) equipped with the monochromatic Al K_α anode radiation source (1486.6 eV) was used to obtain the XPS spectra of ZrMZ and HA-ZrMZ-2, which were further used to determine the semi-quantitative chemical composition and surface chemical states of ZrMZ and HA-ZrMZ-2. The C 1-s signal of an adventitious carbon was used as reference at a binding energy of 284.8 eV. A nonlinear least squares curve fitting program (XPSPEAK41 software) was employed to fit the peak of XPS spectra.

Batch adsorption experiments

Batch adsorption experiments were carried out to study the influence of contact time, initial P concentration, reaction temperature, ionic strength, solution pH, and coexisting electrolyte concentration on the adsorption of phosphate on ZrMZ, HA-ZrMZ-1, and HA-ZrMZ-2.

Adsorption kinetics

To investigate the adsorption kinetics, 15 mg of adsorbent was added into 100-mL conical flask, and 25 mL of 3 mg P/L phosphate solution (pH 7) was also added into this conical flask. Then, the conical flask was transferred into a temperature controlled shaker and shaken at 25 °C and 150 rpm for predefined contact time. After that, the aqueous sample was filtered quickly, and the residual concentration of P in the filtrate was determined on a UV-Vis spectrometry by using the molybdenum blue method with a detecting wavelength of 700 mm. The phosphate adsorption capacity for adsorbent at any time t was calculated according to Eq. (1):

$$q_t = \frac{(C_0 - C_t)V}{m} \tag{1}$$

where q_t (mg P/g) is the phosphate adsorption capacity for adsorbent at any time t; C_0 and C_t are the concentrations of phosphate in solution at initial time and at any time t, respectively (mg P/L); m (g) is the weight of the adsorbent; and V (L) is the volume of phosphate solution.

Adsorption isotherm

To investigate the adsorption isotherm, an exact 15 mg of adsorbent was added into 50 mL of phosphate solution with initial P concentration of 0.2–4.0 mg/L (pH 7). The suspension was then shaken in a temperature-controlled shaker at 25 °C and 150 rpm for 24 h. After that, the adsorbent particles were removed by centrifugation and the residual concentration of P in the supernatant was determined spectrophotometrically. The amount of phosphate adsorbed per unit weight of adsorbent at equilibrium was calculated according to Eq. (2):

$$q_e = \frac{(C_0 - C_e)V}{m} \tag{2}$$

where q_e (mg P/g) is the amount of adsorbed phosphate per unit weight of adsorbent at equilibrium, C_0 (mg P/L) is the initial phosphate concentration, C_e (mg P/L) is the equilibrium concentration, V (L) is the volume of phosphate solution, and m (g) is the weight of the adsorbent.

Effect of temperature, ionic strength, pH, and coexisting electrolyte on adsorption

The effect of temperature was studied by shaking 15 mg of adsorbent in 50 mL of phosphate solutions with an initial concentration of 4 mg P/L (pH 7) at 15, 25, and 35 °C for 24 h, respectively. The effect of ionic strength was studied by shaking 15 mg of adsorbent in 50 mL of solutions with different concentrations of NaCl (0, 10, 50, 200, 400, and 600 mmol/L) and an initial phosphate concentration of 3 mg P/L (pH 7) at 25 °C for 24 h. The effect of pH was studied by shaking 15 mg of adsorbent in 50 mL of 3 mg P/L phosphate solutions with different pH values (3, 4, 5, 6, 7, 8, 9, 10, and 11) at 25 °C for 24 h. The effect of coexisting electrolyte was studied by shaking 15 mg of adsorbent in 50 mL of solutions with an initial electrolyte concentration of 0 or 2 mmol/L and an initial phosphate concentration of 3 mg P/L (pH 7) at

25 °C for 24 h. After equilibrium, the adsorbent particles were removed by centrifugation. The residual phosphate concentration was determined spectrophotometrically, and the amount of phosphate adsorbed per unit mass of adsorbent was calculated according to Eq. (2).

The ^{31}P NMR analyses of ZrMZ and HA-ZrMZ after phosphate adsorption

Solid-state ^{31}P magnetic angle spinning (MAS) NMR spectrometer (Avance III 400 MHz, Bruker Corporation, Germany) was used to measure ^{31}P NMR spectra of phosphate-adsorbed ZrMZ and phosphate-adsorbed HA-ZrMZ-2. The ^{31}P chemical shifts are calibrated using external KH_2PO_4.

Results and discussion

Characterization of ZrMZ and HA-ZrMZ

EDX spectra

The EDX spectra of ZrMZ, HA-ZrMZ-1, and HA-ZrMZ-2 are reported in Fig. 1. The weight percentage (wt%) of elements present in ZrMZ, HA-ZrMZ-1, and HA-ZrMZ-2 determined by EDX are also represented in Fig. 1. The EDX analysis results showed that the major elemental composition on the ZrMZ surface were Si, Al, Zr, O, Fe, K, Na, Ca, Mg, and C, whose weight percentages were 22.36, 6.32, 8.28, 51.88, 1.61, 1.04, 1.46, 1.01, 0.27, and 5.64%, respectively. Zr element was present on the ZrMZ surface (Fig. 1), but it was absent on the surface of the original zeolite (Yang et al. 2015), confirming the loading of zirconium oxides/hydroxides in ZrMZ after the modification of the original zeolites with zirconium. Compared with the weight percentage of C element in ZrMZ, the weight percentage of C element in HA-ZrMZ-1 and HA-ZrMZ-2 markedly increased (Fig. 1), suggesting the occurrence of HA loaded onto the ZrMZ surface after the contact of ZrMZ with HA solution.

Elemental analysis

The contents of carbon and nitrogen in HA, ZrMZ, HA-ZrMZ-1, and HA-ZrMZ-2 determined by elemental analyzer are reported in Table 1. It was shown that the contents of C and N were in the following order: HA > HA-ZrMZ-2 > HA-ZrMZ-1 > ZrMZ, validating that HA had been successfully loaded on the ZrMZ surface after the contact of ZrMZ with HA solution. According to the contents of C in HA, ZrMZ, HA-ZrMZ-1, and HA-ZrMZ-2, the loading amounts of HA in HA-ZrMZ-1 and HA-ZrMZ-2 were determined to be 2.42 and 7.79 mg/g, respectively. It was obvious that the loading amount of HA in HA-ZrMZ-2 was much higher than that in HA-ZrMZ-1.

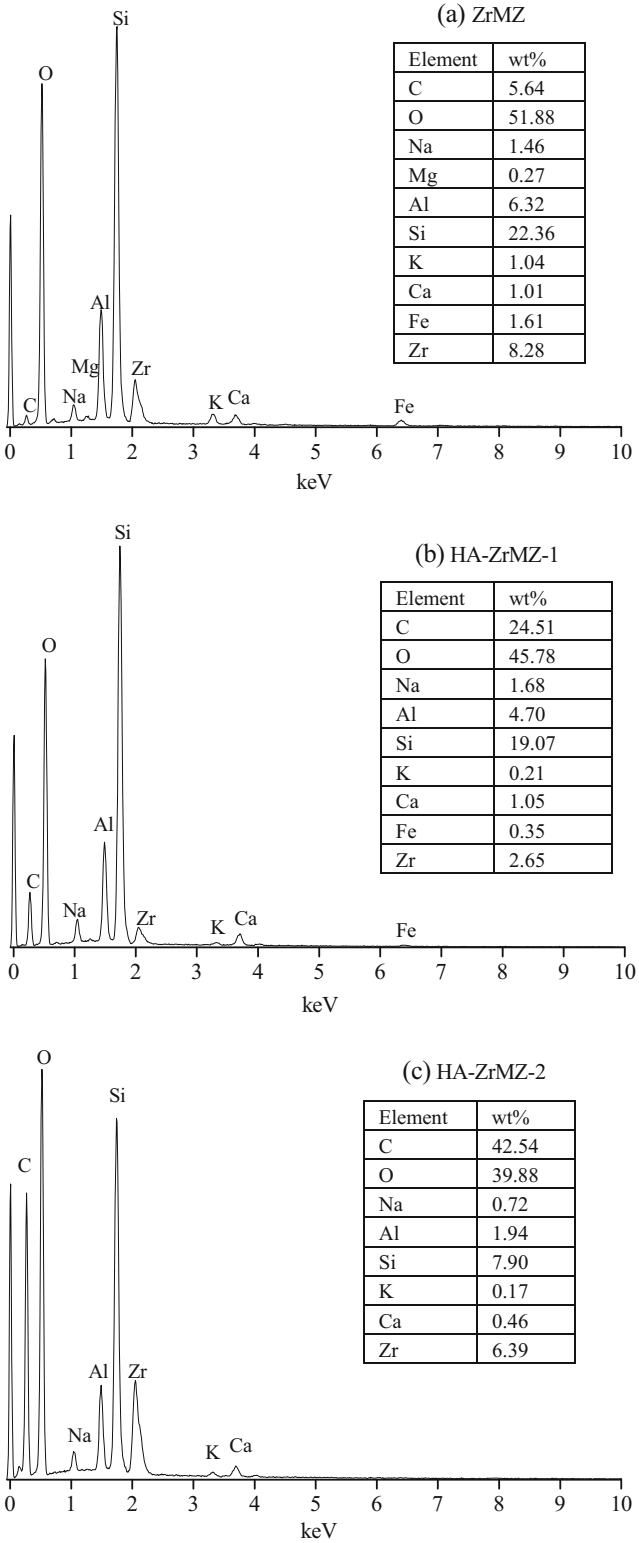

Fig. 1 EDX spectra and surface elemental compositions of **a** ZrMZ, **b** HA-ZrMZ-1, and **c** HA-ZrMZ-2

Table 1 Carbon and nitrogen contents of humic acid, ZrMZ, HA-ZrMZ-1, and HA-ZrMZ-2

Element	Humic acid	ZrMZ	HA-ZrMZ-1	HA-ZrMZ-2
C	37.23%	0.35%	0.44%	0.64%
N	0.81%	0.00%	0.02%	0.04%

N_2 adsorption/desorption isotherms

The N_2 adsorption/desorption isotherms and corresponding BJH pore diameter distributions plots for the original zeolite, ZrMZ, HA-ZrMZ-1, and HA-ZrMZ-2 are presented in Fig. 2. It was shown that the N_2 adsorption took place at a relative pressure less than 0.995 P/P_0. In comparison, the amounts of N_2 adsorbed on ZrMZ at different relative pressures were higher than those of the original zeolite, and also higher than those of HA-ZrMZ (e.g., HA-ZrMZ-1 and HA-ZrMZ-2); especially, the N_2 adsorption capacity for ZrMZ was obviously higher than those for the original zeolite, HA-ZrM-1, and HA-ZrMZ-2 at the relatively pressure of 0.450–0.995 P/P_0. Additionally, the N_2 adsorption/desorption isotherm shapes of the original zeolite, ZrMZ, HA-ZrMZ-1, and HA-ZrMZ-2 were similar, and all these isotherms showed an obvious hysteresis loop at a relative pressure of 0.450–0.995 P/P_0.

The BET surface areas of the original zeolite, ZrMZ, HA-ZrMZ-1, and HA-ZrMZ-2, as calculated from the N_2 adsorption isotherm data, were found to be 19.0185, 71.8310, 56.2882, and 50.6104 m^2/g, respectively. According to the N_2 adsorption isotherm data, the total pore volumes of the original zeolite, ZrMZ, HA-ZrMZ-1, and HA-ZrMZ-2 were calculated to be 0.033406, 0.067646, 0.0048469, and 0.049404 cm^3/g, respectively. It was obvious that the surface area and pore volume of ZrMZ were much higher than those of the original zeolite, suggesting that the ZrMZ could be more suitable to be used as an adsorbent for removing pollutants from aqueous solution than the original zeolite. The increase of BET surface area and total pore volume after zirconium modification might be attributed to the fact that the loaded zirconium oxide particles on the zeolite surface provided a higher surface area and a higher pore volume than the original zeolite (Chitrakar et al. 2006; Zong et al. 2016). Moreover, the

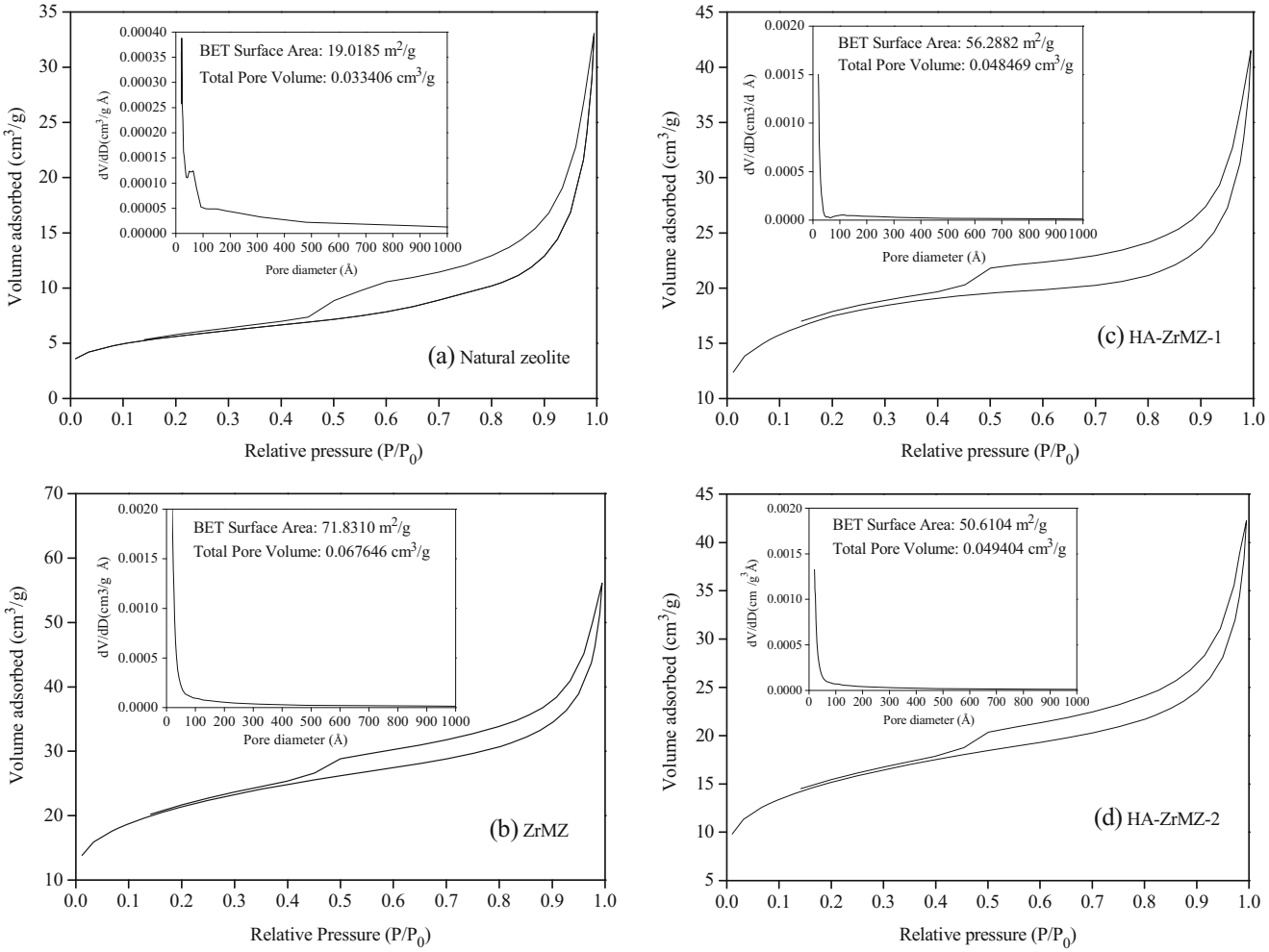

Fig. 2 N_2 adsorption/desorption isotherm of **a** natural zeolite, **b** ZrMZ, **c** HA-ZrMZ-1, and **d** HA-ZrMZ-2

surface areas and pore volumes of HA-ZrMZ-1 and HA-ZrMZ-2 were less than those of ZrMZ, reflecting that the coating of HA can decrease both the surface area and pore volume of ZrMZ. Similar trend of HA coating effect on the surface area has been observed for iron oxide (Wang et al. 2015b; Yan et al. 2016).

According to the classification of pore size made by the International Union of Pure and Applied Chemistry (IUPAC), the diameters of micropores, mesopores, and macropores are less than 2 nm, between 2 and 50 nm, and more than 50 nm, respectively. In the N_2 adsorption isotherm, the relative pressure less than 0.1 P/P_0 was related to micropores, 0.1–0.8 P/P_0 was related to mesopores, while 0.8–10 P/P_0 was related to macropores (Wang et al. 2015a). The N_2 adsorption/desorption isotherms of the original zeolite, ZrMZ, HA-ZrMZ-1, and HA-ZrMZ-2 all were categorized as type IV isotherm with a distinct hysteresis loop observed in the range of 0.45–0.99 P/P_0, indicative of the presence of abundant mesopores in the original zeolite, ZrMZ, HA-ZrMZ-1, and HA-ZrMZ-2 (Zhang et al. 2012). Furthermore, it was seen that the hysteresis loop shifted approach relative pressure $(P/P_0) = 1$, suggesting the existence of macropores in the original zeolite, ZrMZ, HA-ZrMZ-1, and HA-ZrMZ-2 (Zhang et al. 2012). These results were in good agreement with the BJH pore diameter distributions of the original zeolite, ZrMZ, HA-ZrMZ-1, and HA-ZrMZ-2. The significant decrease of the N_2 adsorption capacity at the relative pressure of 0.450–0.995 P/P_0 demonstrates that the decrease of pore volume can be attributed to the decrease of mesopore and macropore volumes.

Point of zero charge

As shown in Fig. 3, the pH_{PZC} values of ZrMZ, HA-ZrMZ-1, and HA-ZrMZ-2 were 7.73, 7.23, and 6.85, respectively. The surface charges of ZrMZ, HA-ZrMZ-1, and HA-ZrMZ-2 were highly dependent upon solution pH. When solution pH is below pH_{PZC}, the surface charges of ZrMZ, HA-ZrMZ-1, and HA-ZrMZ-2 are positive, which is beneficial for the adsorption of the negatively charged phosphate anions. However, when solution pH is above pH_{PZC}, the surface charges of ZrMZ, HA-ZrMZ-1, and HA-ZrMZ-2 are negative. In this case, a barrier will be created by the electrostatic repulsion interaction between the negatively charged adsorbent and the negatively charged phosphate anion, which will inhibit the adsorption of phosphate anions on the negatively charged adsorbent.

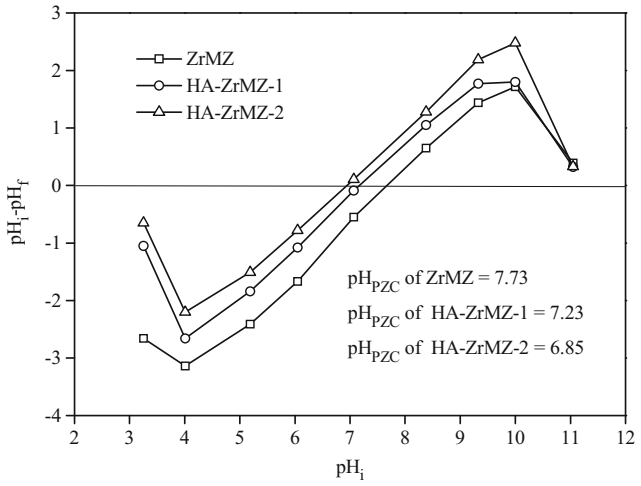

Fig. 3 Determination of pH_{PZC} of ZrMZ, HA-ZrMZ-1, and HA-ZrMZ-2

Two principal adsorption mechanisms have been proposed for HA adsorption onto metal oxides, i.e., electrostatic attraction and ligand exchange (Liu et al. 2014; Sun and Lee 2012). At solution pH 7, the HA molecules could be considered as anions and they were partially negatively charged because carboxylic groups of HA usually dissociates at pH >4, whereas phenolic groups of HA usually dissociates at pH >8 (Sun and Lee 2012). The ZrMZ surface was positively charged at solution pH 7 (Fig. 3). Therefore, at solution pH 7, the negatively charged HA would be adsorbed on the positively charged ZrMZ surface due to the electrostatic attraction. The occurrence of specific chemical reaction between the adsorbent surface and the adsorbate can change the surface charge of the adsorbent, but there is no change in the surface charge of adsorbent when no specific chemical reaction between the adsorbent surface and the adsorbate takes place (Chen et al. 2013; Su et al. 2013). Therefore, the formation of outer-sphere complexes on the adsorbent surface cannot change the pH_{PZC} value of the adsorbent, but inter-sphere complex formation can change the pH_{PZC} value (Chen et al. 2013; Su et al. 2013). The decrease in the pH_{PZC} value of ZrMZ induced by HA coating could be attributed to the formation of anionic negatively charged inner-sphere surface complexes via a ligand exchange process (Chen et al. 2013). Therefore, the decrease of pH_{PZC} demonstrated that the specific chemical reaction rather than the purely electrostatic attraction existed between the HA molecules and the ZrMZ surface to form anionic negatively charged inner-sphere surface complexes. Thus, it was proposed that the interaction between HA and ZrMZ at solution pH 7 was firstly initiated by the electrostatic attraction between the negatively charged HA and the positively charged ZrMZ surface, and then, the hydroxyl groups of ZrMZ (e.g., Zr-OH and Zr-OH_2^+) interacted with the deprotonated functional groups of HA (e.g., $-COO^-$) via a ligand exchange process to form surface complexes. Similar adsorption mechanisms have been proposed for HA adsorption onto TiO_2 microsphere (Sun and Lee 2012) at solution pH below their pH_{PZC} values. The suggested mechanisms for the interaction of ZrMZ with HA will be proven conclusively by the analysis of XPS spectra in the "XPS spectra" section.

XPS spectra

XPS is a useful tool for determining the composition of adsorbents as well as the chemical state of elements on the adsorbent surface. Figure 4a shows the wide scan XPS spectra of ZrMZ and HA-ZrMZ-2. The presence of the peaks of Al 2p, Si 2 s, Zr 3d, O 1 s, and Na 1 s in the XPS wide scan spectra of ZrMZ and HA-ZrMZ-2 indicates that the ZrMZ and HA-ZrMZ-2 contain Al, Si, Zr, O, and Na. The presence of the C 1-s peak in the XPS spectrum of ZrMZ was attributed to the adventitious carbon used for calibrating the binding energy which did not change during adsorption. The presence of the C 1-s peak in the XPS spectrum of HA-ZrMZ-2 was attributed to the adventitious carbon or both the adsorbed HA and adventitious carbon.

Figure 4b, c shows the decomposition of high-resolution scan of O 1-s XPS spectra for ZrMZ and HA-ZrMZ-2, respectively. As shown in Fig. 4b, the high-resolution scan of O 1-s XPS spectrum for ZrMZ could be divided into three component peaks of the O species in the form of metal oxide (O^{2-}), hydroxyl group bonded to metal (−OH), and adsorbed water (H_2O), whose binding energy (BE) values were 530.52, 531.71, and 532.57 eV, respectively. As shown in Fig. 4c, the high-resolution scan of O 1-s XPS spectrum for HA-ZrMZ-2 could be divided into four component peaks of the O species in the form of O^{2-}, carboxylic functional groups ($-COO^-$), −OH, and H_2O, whose BE values were 530.16, 531.14, 531.98, and 532.93 eV, respectively. A peak assigned to O in carboxylic functional groups was found in the high-resolution scan of O 1-s XPS spectrum of HA-ZrMZ-2, demonstrating that HA had been successfully loaded on the ZrMZ surface after the contact of ZrMZ with HA solution. The fitting parameters of different O 1-s peaks for ZrMZ and HA-ZrMZ-2 are summarized in Table 2. It was shown that the −OH percentages for ZrMZ and HA-ZrMZ-2 were 55.35 and 43.70%, respectively. This demonstrated that large amounts of hydroxyl groups existed on the surface of ZrMZ and HA-ZrMZ-2, which were beneficial for the adsorption of phosphate through a ligand exchange mechanism.

The high-resolution scan of Zr 3d spectra for ZrMZ and HA-ZrMZ-2 are presented in Fig. 4d. It was shown that the binding energy of Zr 3d was shifted to the higher value after

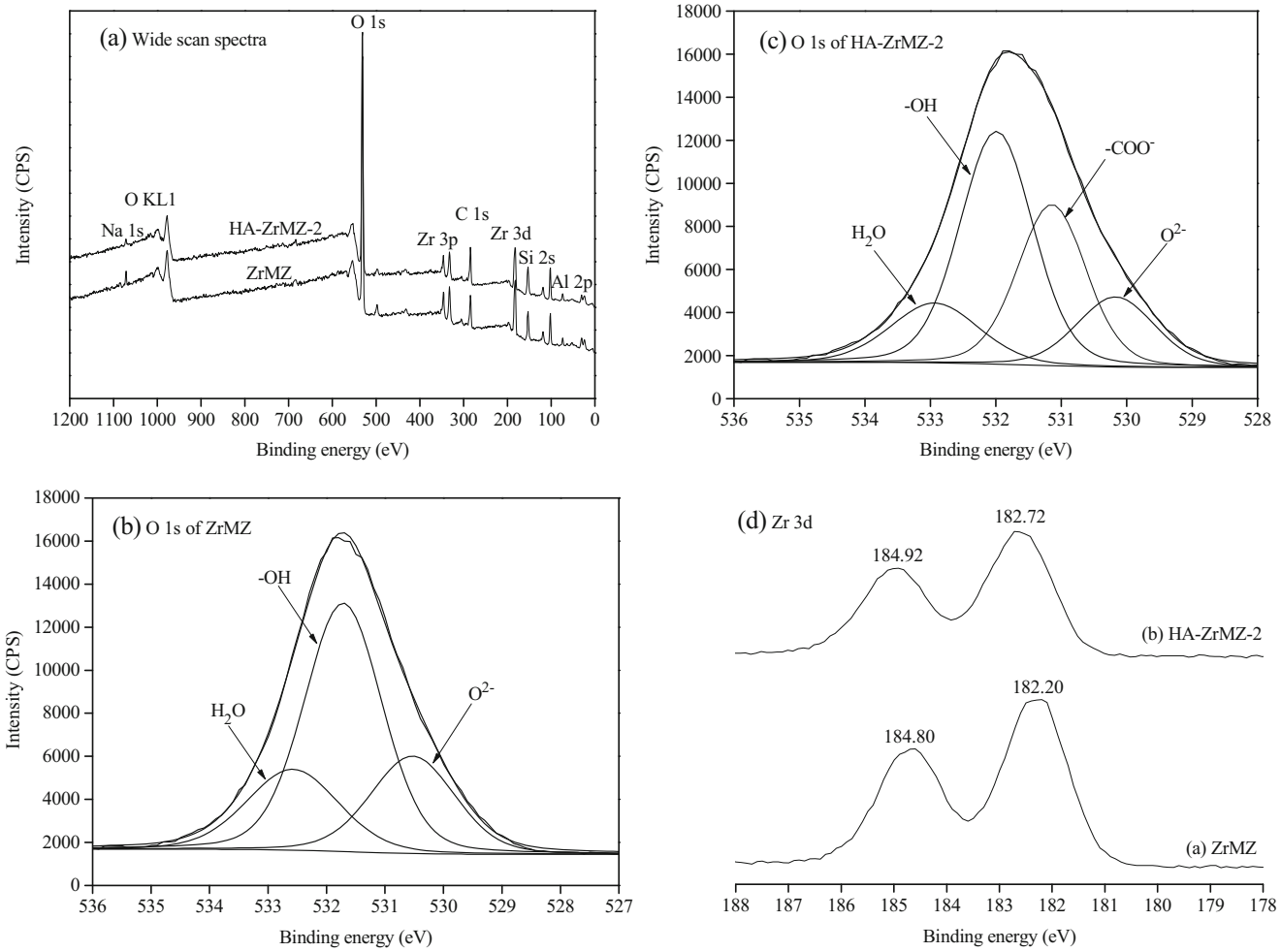

Fig. 4 XPS spectra of ZrMZ and HA-ZrMZ-2. **a** Wide scan spectra. **b** O 1-s spectrum of ZrMZ. **c** O 1-s spectrum of HA-ZrMZ-2. **d** Zr 3d spectra

Table 2 Fitting parameters of O 1-s peak of ZrMZ and HA-ZrMZ-2

Samples	Peak	Binding energy (eV)	FWHM	Area	Percentage (%)
ZrMZ	H_2O	532.57	1.85	8,088.75	21.20
	−OH	531.71	1.57	21,123.97	55.35
	O^{2-}	530.52	1.70	8,949.97	23.45
HA-ZrMZ-2	H_2O	532.93	1.60	5,176.05	13.66
	−OH	531.98	1.31	16,552.41	43.70
	$-COO^-$	531.14	1.24	10,815.61	28.55
	O^{2-}	530.16	1.41	5,335.99	14.09

the coating of HA on ZrMZ, suggesting that the Zr element in the ZrMZ took part in the HA coating process. Before the HA coating, great amounts of hydroxyl groups existed on the surface of zirconium oxides in ZrMZ. Previous studies have shown that the functional carboxylic groups (−COOH) and phenolic hydroxyl groups (−OH) of HA are considered to be active and can interact with the surfaces of many metal oxides (Sun and Lee 2012; Yan et al. 2016; Zhou et al. 2015). At solution pH 7, the dissociation of carboxylic groups is expected to occur, whereas the dissociation of phenolic hydroxyl groups does not occur (Sun and Lee 2012). Therefore, the carboxylic group would play an important role in the coating of HA on the ZrMZ surface at solution pH 7. After the HA coating, the hydroxyl groups bounded to Zr (i.e., Zr–OH and $Zr–OH_2^+$) would be partially replaced by the deprotonated functional carboxylic groups ($-COO^-$) of HA via a ligand exchange process and the surface inner-sphere complexes (i.e., Zr–O–C(O)) would be formed. The reaction between ZrMZ and HA molecules could be described as follows (Sun and Lee 2012):

$$HA{-}COOH = HA{-}COO^- + H^+ \quad (3)$$

$$Zr{-}OH + HA{-}COO^- = Zr{-}O{-}C(O){-}HA + OH^- \quad (4)$$

$$Zr{-}OH_2^+ + HA{-}COO^- = Zr{-}O{-}C(O){-}HA + H_2O \quad (5)$$

Due to the fact that the electronegativity value of C was higher than that of H, the negative charge density of Zr in Zr–O–C(O) was lower than that in Zr–O–H, leading to an increase in the binding energy of Zr 3d in ZrMZ after the HA coating. Therefore, the results obtained from the analysis of Zr 3d spectra confirmed the formation of Zr–O–C(O) bond on the ZrMZ surface.

Adsorption kinetics

The time-resolved adsorption curves of phosphate on ZrMZ, HA-ZrMZ-1, and HA-ZrMZ-2 are depicted in Fig. 5. It was shown that the adsorption kinetic processes of phosphate on ZrMZ, HA-ZrMZ-1, and HA-ZrMZ-2 were divided into two stages: (i) an initial fast adsorption stage in which most (more than 80%) of phosphate was adsorbed within the first 6 h of contact and (ii) a slow adsorption stage in which the adsorption slowly reached an equilibrium stage with the increase of contact time after 6 h. Furthermore, the amount of phosphate adsorbed on HA-ZrMZ-1 or HA-ZrMZ-2 was lower than that on ZrMZ under the condition of the same reaction time, indicating that the preloading of HA inhibits the phosphate adsorption. In addition, the amount of adsorbed phosphate on HA-ZrMZ-2 was lower than that on HA-ZrMZ-1, indicating that the more the HA preloading amount is, the less the phosphate adsorption capacity is.

In an attempt to further evaluate the adsorption kinetics, the pseudo-second-order kinetic model was used to fit the kinetic data. The linear form of pseudo-second-order kinetic model is described as Eq. (6) (Ho and McKay 1999):

$$\frac{t}{q_t} = \frac{t}{q_e} + \frac{1}{k_2 q_e^2} \quad (6)$$

where q_t (mg/g) and q_e (mg/g) are the phosphate adsorption capacity for adsorbent at any time t and at equilibrium, respectively, and k_2 (g/(mg min)) is the rate constant of pseudo-second-order kinetic model adsorption. If the pseudo-second-order kinetic model gives a good fit to the kinetic data, the plot of t/q_t against t should provide a linear relationship. The values of q_e and k_2 were determined from the slope and

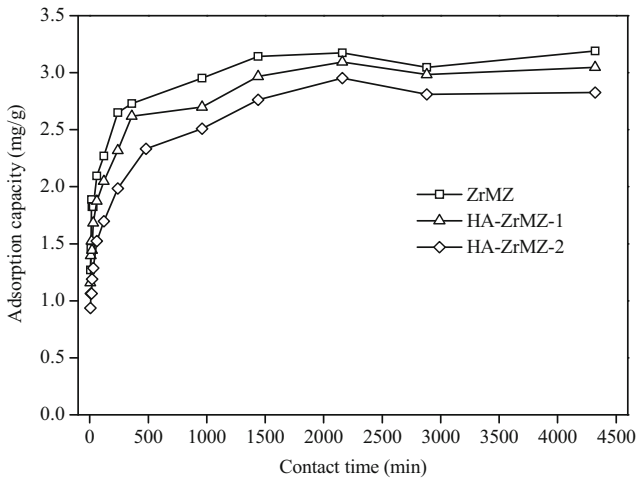

Fig. 5 Adsorption kinetics of phosphate on ZrMZ, HA-ZrMZ-1, and HA-ZrMZ-2

Table 3 Pseudo-second-order and intra-particle diffusion kinetic model parameters for phosphate adsorption onto ZrMZ, HA-ZrMZ-1, and HA-ZrMZ-2

Samples	Pseudo-second-order kinetic model					Intra-particle diffusion model		
	$q_{e,2}$ (mg/g)	k_2 (g/mg min)	h (mg/g min)	$t_{1/2}$ (min)	R^2	k_p (mg/g min$^{0.5}$)	C_i (mg/g)	R^2
ZrMZ	3.18	0.00999	0.101	31.5	0.999	0.0645	1.57	0.969
HA-ZrMZ-1	3.06	0.00798	0.0749	40.9	0.999	0.0743	1.21	0.980
HA-ZrMZ-2	2.87	0.00653	0.0539	53.3	0.999	0.0689	0.889	0.981

intercept of the linear plot of t/q_t against t. The calculated q_e and k_2 were further used to calculate the initial adsorption rate h (mg/(g min)) and half-adsorption time $t_{1/2}$ (min) according to Eqs. (7) and (8), respectively (Pan et al. 2009):

$$h = k_2 q_e^2 \tag{7}$$

$$t_{1/2} = \frac{1}{k_2 q_e} \tag{8}$$

where q_e (mg/g) is the phosphate adsorption capacity for adsorbent at equilibrium and k_2 (g/(mg min)) is the rate constant of pseudo-second-order kinetic model adsorption.

The calculated parameter values of pseudo-second-order model along with the correlation coefficients (R^2) are represented in Table 3. The very high values of R^2 indicated the good applicability of the pseudo-second-order kinetic model to describe the adsorption kinetic process, suggesting that the adsorption of phosphate on ZrMZ and HA-ZrMZ is a chemical sorption process which involves valency forces through exchange or sharing of electrons between ZrMZ and phosphate, i.e., the replacement of surface hydroxyl groups by phosphate anions to form inner-sphere phosphate complexes on the ZrMZ surface. This conclusion will be further discussed in the adsorption mechanism studies in the following sections including isotherm, ionic strength effect, and ^{31}P NMR studies. The h values of HA-ZrMZ-1 and HA-ZrMZ-2 were lower than that of ZrMZ, while the $t_{1/2}$ values of HA-ZrMZ-1 and HA-ZrMZ-2 were higher than that of ZrMZ, indicating that the preloading of HA on ZrMZ can reduce the phosphate adsorption rate. Furthermore, the h value of HA-ZrMZ-2 was lower than that of HA-ZrMZ-1, while the $t_{1/2}$ value of HA-ZrMZ-2 was higher than that of HA-ZrMZ-1, indicating that the ZrMZ with more HA loading amount exhibits a lower phosphate adsorption rate. The HA coating would block the internal pores of adsorbents, thereby resulting in the reduction of the phosphate adsorption rate (Wang et al. 2015b).

The adsorption kinetics of phosphate from aqueous solution on ZrMZ and HA-ZrMZ in a well-mixed batch system consists of three consecutive steps: (i) film diffusion of phosphate from the bulk solution through the boundary layer to the surface of the adsorbent, (ii) intra-particle diffusion of phosphate into the internal pore of the adsorbent, and (iii) phosphate adsorption at sites. To identify whether or not the intra-particle diffusion is the rate-controlled step, the Weber and Morris intra-particle diffusion model was applied to analyze the kinetic data. The intra-particle diffusion model given by Weber and Morris is described as follow (Weber and Morris 1964):

$$q_t = k_p t^{0.5} + C_i \tag{9}$$

where k_p (mg/(g min$^{0.5}$) is the intra-particle diffusion rate constant and C_i (mg/g) is the constant of the intra-particle diffusion model which is related to the thickness of boundary layer. The larger the C_i value is, the greater the contribution of boundary layer effect to the rate-controlling step is (Gheju et al. 2016). If the intra-particle diffusion is the rate-limited step during the adsorption process, the plot of q_t versus $t^{0.5}$ will be linear. If the intercept of the linear plot of q_t versus $t^{0.5}$ is zero, the rate of adsorption is only controlled by the intra-particle diffusion. If the linear plot of q_t versus $t^{0.5}$ deviates from origin, the intra-particle diffusion is not the sole rate-limited step. The fitted results of the experimental data for phosphate adsorption onto ZrMZ, HA-ZrMZ-1, and HA-ZrMZ-2 are shown in Fig. 6. It was seen that the adsorption

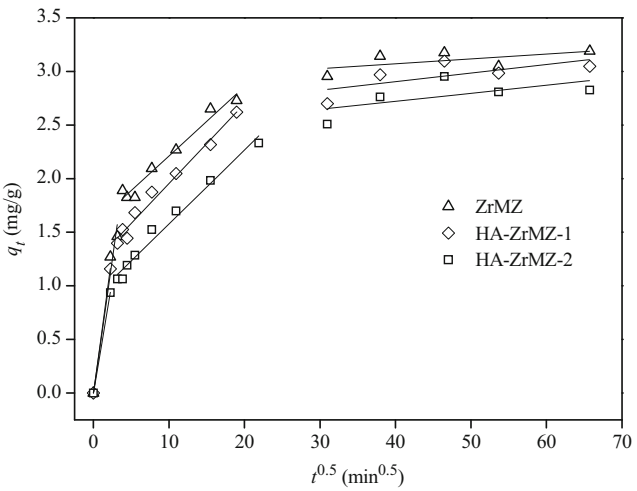

Fig. 6 Intra-particle model for phosphate adsorption onto ZrMZ, HA-ZrMZ-1, and HA-ZrMZ-2

kinetics of phosphate on ZrMZ, HA-ZrMZ-1, and HA-ZrMZ-2 was controlled by three different stages. The first region was the instantaneous external surface adsorption stage, which was related to the film diffusion or boundary layer diffusion. The second region was a gradual adsorption stage where the intra-particle diffusion was the rate-controlled step. The third region was a final equilibrium stage where the intra-particle diffusion began to slow down because of the low phosphate concentration left in the solution as well as the less number of available adsorption sites on the adsorbent surface (Lin et al. 2011a; Liu et al. 2013). The values of k_p and C_i calculated from the slope and intercept of the second portion of q_t versus $t^{0.5}$ plot are shown in Table 3. As shown in Table 3, the intra-particle diffusion was not the sole rate-limited step during the gradual adsorption stage because the intercept of the second port of q_t versus $t^{0.5}$ plots was not zero, and the external diffusion and intra-particle diffusion simultaneously controlled the adsorption of phosphate on ZrMZ, HA-ZrMZ-1, and HA-ZrMZ-2 during the gradual adsorption stage. The C_i values of HA-ZrMZ-1 and HA-ZrMZ-2 were lower than that of ZrMZ, and the C_i value of HA-ZrMZ-2 was lower than that of HA-ZrMZ-1, suggesting that the contribution of film diffusion or boundary layer diffusion to the rate-limiting step during the gradual adsorption process became less important with increasing the HA preloading amount of ZrMZ. A similar result has been found for the effect of HA coating on the kinetics of phosphate adsorption onto ferrihydrite (Wang et al. 2015b).

Adsorption isotherms

The adsorption isotherms of phosphate on ZrMZ, HA-ZrMZ-1, and HA-ZrMZ-2 are given in Fig. 7. As shown in Fig. 7, the amount of phosphate adsorbed on ZrMZ and HA-ZrMZ increased with the increase of the equilibrium phosphate concentration. Furthermore, the amount of phosphate adsorbed on HA-ZrMZ was less than that of ZrMZ, and the amount of phosphate adsorbed on HA-ZrMZ decreased with increasing the HA preloading amount. This indicates that the preloading of HA on ZrMZ inhibits the adsorption of phosphate, and the more the HA loading amount is, the lower the phosphate adsorption capacity is.

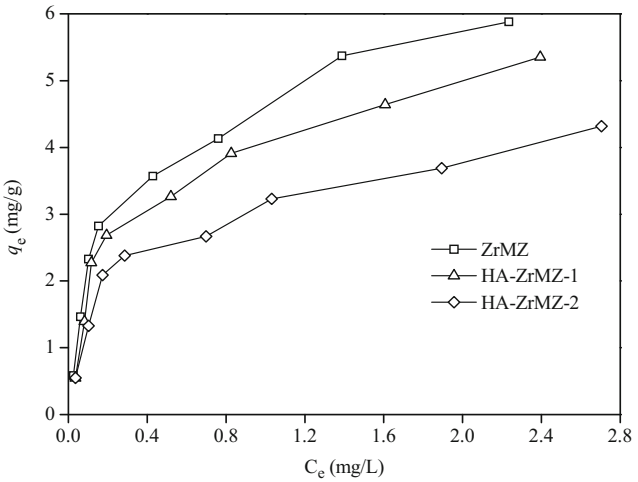

Fig. 7 Adsorption isotherms of phosphate on ZrMZ, HA-ZrMZ-1, and HA-ZrMZ-2

Adsorption isotherm models are commonly used to describe adsorption behaviors as well as study its microscopic adsorption mechanisms. In this study, three widely used isotherm models including Langmuir, Freundlich, and Dubinin-Redushkevich (D-R) models were chosen to fit the adsorption equilibrium experimental data. The nonlinear form of Langmuir isotherm model is expressed as (Langmuir 1916):

$$q_e = \frac{q_m K_L C_e}{1 + K_L C_e} \tag{10}$$

where q_e is the amount of adsorbate adsorbed per unit mass of adsorbent at equilibrium (mg/g), C_e is the concentration of adsorbate in solution at equilibrium (mg/L), q_m is the saturated adsorbate adsorption capacity for adsorbent to form a complete monolayer on the adsorbent surface (mg/g), and K_L is the constant for Langmuir isotherm model which is related to the adsorption energy (L/mg). Furthermore, the K_L value can be used to predict whether the adsorption is favorable or not. A dimensionless separation factor (R_L), which can be applied to express the characteristics of the adsorption isotherm, is defined based on the following equation (Seliem et al. 2016):

$$R_L = \frac{1}{1 + K_L C_0} \tag{11}$$

where K_L is the constant for Langmuir isotherm model (L/mg) and C_0 is the initial adsorbate concentration (mg/L). The value of R_L indicates the favorability of adsorption: (1) $R_L > 1$ for unfavorable adsorption, (2) $R_L = 1$ for linear adsorption, (3) $0 < R_L < 1$ for favorable adsorption, and (4) $R_L = 0$ for irreversible adsorption (Seliem et al. 2016).

The Langmuir fitting results are represented in Table 4. The high correlation coefficients ($R^2 = 0.938$–0.953) suggest that the adsorption isotherms of phosphate onto ZrMZ and HA-ZrMZ can be well described by the Langmuir isotherm model. The R_L values in this study were in the range of 0–1, indicative of favorable adsorption of phosphate on ZrMZ, HA-ZrMZ-1, and HA-ZrMZ-2. The R_L values of HA-ZrMZ-1 and HA-ZrMZ-2 were higher than those of ZrMZ, indicating that phosphate adsorption on HA-ZrMZ appears less favorable than on ZrMZ. The q_m values of ZrMZ and HA-ZrMZ were in the following order: ZrMZ > HA-ZrMZ-1 > HA-ZrMZ-2. This indicates that the preloading of HA on ZrMZ reduces the maximum monolayer phosphate adsorption capacity, and the ZrMZ with a higher HA preloading amount exhibits a lower maximum phosphate adsorption capacity.

Table 4 Isotherm parameters for phosphate adsorption onto ZrMZ, HA-ZrMZ-1, and HA-ZrMZ-2

Isotherm model	Parameter	ZrMZ	HA-ZrMZ-1	HA-ZrMZ-2
Langmuir	q_m (mg/g)	5.96	5.37	4.21
	K_L (L/mg)	4.91	4.43	4.30
	R_L	0.0485–0.505	0.0534–0.530	0.0549–0.538
	R^2	0.953	0.949	0.938
Freundlich	K_F	4.62	4.02	3.11
	$1/n$	0.352	0.350	0.330
	R^2	0.940	0.940	0.943
D-R	q_0 (mg/g)	25.3	22.3	15.9
	K_D (mol^2/kJ^2)	0.00257	0.00258	0.00246
	E (kJ/mol)	13.9	13.9	14.3
	R^2	0.966	0.952	0.954

The nonlinear form of Freundlich isotherm model is expressed as follows (Freundlich 1926):

$$q_e = K_F C_e^{1/n} \quad (12)$$

where q_e is the amount of adsorbate adsorbed per unit mass of adsorbent at equilibrium (mg/g), C_e is the concentration of adsorbate in solution at equilibrium (mg/L), and K_F and $1/n$ are the Freundlich constants which are related to the adsorption capacity of the adsorbent and the adsorption density, respectively. If the value of $1/n$ is in the range of 0.1 to 1, it indicates favorable adsorption of adsorbate on adsorbent (Islam et al. 2013).

The Freundlich fitting results are represented in Table 4. The high correlation coefficients (R^2 = 0.940–0.943) suggest that the Freundlich isotherm model fits well to the adsorption equilibrium experiment data of phosphate on ZrMZ and HA-ZrMZ. The $1/n$ values in this study were between 0.1 and 1, indicative of favorable adsorption of phosphate on ZrMZ, HA-ZrMZ-1, and HA-ZrMZ-2. The values of K_F varied in the following order: ZrMZ > HA-ZrMZ-1 > HA-ZrMZ-2, suggesting that the preloading of HA on ZrMZ reduces the phosphate adsorption capacity, and the ZrMZ with a higher HA preloading amount exhibits a lower phosphate adsorption capacity.

The nonlinear form of D-R isotherm model can be written as (Lin et al. 2011a)

$$q_e = q_0 \exp\left(-K_D \varepsilon^2\right) \quad (13)$$

where q_e is the amount of adsorbate adsorbed per unit mass of adsorbent at equilibrium (mg/g), q_0 is the maximum adsorbate adsorption capacity for adsorbent (mg/g), and ε is the Polanyi potential, and it is equal to $RT\ln(1 + 1/C_e)$, where C_e is the concentration of adsorbate in solution at equilibrium (mol/L), R is the universal gas constant (kJ/(mol K)), T is the temperature of adsorption reaction (K), and K_D is the constant for D-R isotherm model related to the mean free energy of adsorption (mol^2/kJ^2). The mean free energy of adsorption (E; kJ/mol) can be calculated as follows (Lin et al. 2011a):

$$E = \frac{1}{\sqrt{2K_D}} \quad (14)$$

The magnitude of E can predict the adsorption mechanism, i.e., physical or chemical adsorption. If the E value is below 8 kJ/mol, the adsorption process is physical in nature, and if the E value is higher than 8 kJ/mol, the adsorption type is a chemical adsorption (D'Arcy et al. 2011).

The D-R fitting results are represented in Table 4. The high correlation coefficients (R^2 = 0.952–0.966) indicates that the adsorption isotherms of phosphate on ZrMZ and HA-ZrMZ can be fitted well by the D-R isotherm model. The E values obtained from this study were 13.9, 13.9, and 14.3 kJ/mol for ZrMZ, HA-ZrMZ-1, and HA-ZrMZ-2, respectively, which were all higher than 8 kJ/mol. This indicates that the adsorption of phosphate on ZrMZ, HA-ZrMZ-1, and HA-ZrMZ-2 is a chemisorption process rather than a physical adsorption process. This conclusion is in accordance with that made from the kinetic study.

Effect of temperature on phosphate adsorption and thermodynamic parameters

Figure 8 shows the effect of temperature on the adsorption of phosphate on ZrMZ, HA-ZrMZ-1, and HA-ZrMZ-2. As shown in Fig. 8, the amounts of phosphate adsorbed on ZrMZ, HA-ZrMZ-1, and HA-ZrMZ-2 increased with increasing reaction temperature, indicating favorable adsorption process at higher temperature. Furthermore, the amount of phosphate adsorbed on HA-ZrMZ-1 or HA-ZrMZ-2 at different reaction temperatures was less than that of ZrMZ (Fig. 8), indicating that HA preloading onto ZrMZ reduces the phosphate adsorption. In addition, the amount of phosphate adsorbed on HA-ZrMZ-2 was less than that of HA-ZrMZ-1,

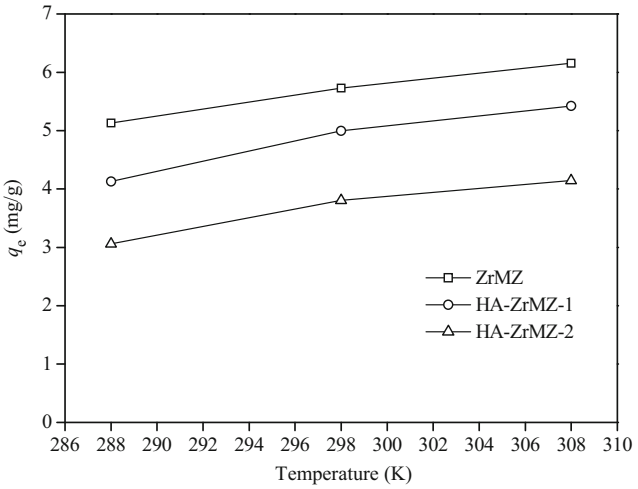

Fig. 8 Effect of temperature on phosphate adsorption onto ZrMZ, HA-ZrMZ-1, and HA-ZrMZ-2

indicating that the more the HA preloading is, the less the phosphate adsorption capacity is.

The thermodynamic parameters, including Gibbs free energy of adsorption ($\triangle G°$), enthalpy change ($\triangle H°$), and entropy change ($\triangle S°$), were calculated by using the experimental data of phosphate adsorption onto ZrMZ and HA-ZrMZ at 288, 298, and 308 K. The equilibrium constant K_c (mL/g) can be calculated using Eq. (15) (Lu et al. 2015):

$$K_c = \frac{q_e}{C_e} \tag{15}$$

where q_e (mg/g) is the amount of phosphate adsorbed per unit mass of adsorbent at equilibrium and C_e (mg/mL) is the concentration of phosphate in aqueous solution at equilibrium. The values of $\triangle G°$ at different temperatures can be calculated using Eq. (16) (Gheju et al. 2016; Lu et al. 2015):

$$\Delta G^{\circ} = -RT\ln(K_c) \tag{16}$$

where K_c is the adsorption equilibrium constant, R (8.314 J/(mol K)) is the universal gas constant, and T (K) is the temperature of adsorption reaction. The values of $\triangle H°$ and $\triangle S°$ can be calculated from the slope and intercept of the linear plot of $\ln(K_c)$ versus $1/T$ as follows (Lu et al. 2015):

$$\ln(K_c) = \frac{\Delta S^{\circ}}{R} - \frac{\Delta H^{\circ}}{RT} \tag{17}$$

The calculated thermodynamic parameters are given in Table 5. The values of $\triangle G°$ at different temperatures were negative, suggesting the spontaneous nature of phosphate adsorption onto ZrMZ, HA-ZrMZ-1, and HA-ZrMZ-2. The decrease of $\triangle G°$ with an increase in reaction temperature implies the increase of spontaneity at higher temperatures. The values of $\triangle H°$ are positive, revealing that the adsorption of phosphate on ZrMZ, HA-ZrMZ-1, and HA-ZrMZ-2 is endothermic in nature and the adsorbed amount at equilibrium increases with increasing temperature. The positive values of $\triangle S°$ suggest that the adsorption of phosphate on ZrMZ, HA-ZrMZ-1, and HA-ZrMZ-2 results in an increased disorder at the solid/liquid interface.

Table 5 Thermodynamic parameters for phosphate adsorption onto ZrMZ, HA-ZrMZ-1, and HA-ZrMZ-2

Samples	ΔG° (kJ/mol)			ΔH° (kJ/mol)	ΔS° (J/(mol · K))
	288 K	298 K	308 K		
ZrMZ	−18.3	−19.4	−20.4	11.6	104
HA-ZrMZ-1	−17.5	−18.8	−19.8	15.7	115
HA-ZrMZ-2	−16.5	−17.8	−18.7	15.4	111

Effect of ionic strength on phosphate adsorption

To further explore the microscopic mechanisms for phosphate adsorption onto ZrMZ, HA-ZrMZ-1, and HA-ZrMZ-2, the effect of ionic strength on the phosphate adsorption was evaluated in this study. The ionic strength was adjusted by adding different amounts of NaCl into the phosphate solution. The effect of ionic strength on phosphate adsorption onto ZrMZ, HA-ZrMZ-1, and HA-ZrMZ-2 is presented in Fig. 9. At low ionic strength, an increase in ionic strength from 0 to 50 mmol/L enhanced the adsorption of phosphate on ZrMZ, HA-ZrMZ-1, and HA-ZrMZ-2, while further increasing ionic strength did not result in a further increase of the phosphate adsorption capacity (Fig. 9). This indicates that the adsorption of phosphate on ZrMZ, HA-ZrMZ-1, and HA-ZrMZ-2 is enhanced by ionic strength.

Two main adsorption processes including outer-sphere complex formation and inner-sphere complex formation have been suggested for phosphate adsorption onto metal oxides

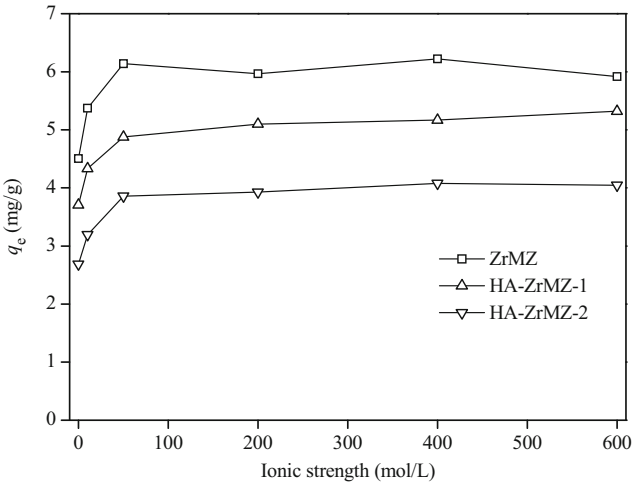

Fig. 9 Effect of ionic strength on phosphate adsorption onto ZrMZ, HA-ZrMZ-1, and HA-ZrMZ-2

(Wang et al. 2016b). The former involves the purely electrostatic attraction interaction between the negatively charged phosphate anion and the positively charged metal oxide surface, while the latter involves a ligand exchange process between adsorbent and adsorbate (Wang et al. 2016b). It is well known that a strongly negative influence of ionic strength on phosphate adsorption is typical for outer-sphere complexation rather than inner-sphere complexation (Liu et al. 2008; Su et al. 2013; Su et al. 2015). If phosphate formed outer-sphere surface complexes at the solid/liquid interface, the phosphate adsorption capacity would decrease with increasing ionic strength (Liu et al. 2008; Su et al. 2013; Su et al. 2015). However, if phosphate formed inner-sphere surface complexes at the solid/liquid interface, the phosphate adsorption capacity would either increase or not change with increasing ionic strength (Liu et al. 2008; Su et al. 2013; Su et al. 2015). The results obtained from Fig. 9 suggested that the adsorption of phosphate on ZrMZ, HA-ZrMZ-1, and HA-ZrMZ-2 at solution pH 7 mainly obeyed the inner-sphere complex mechanism rather than the purely electrostatic attraction mechanism. The increased phosphate adsorption for ZrMZ and HA-ZrMZ by ionic strength could be due to the fact that the negatively charged complexes formed by the adsorption of phosphate via an inner-sphere complexation mechanism could be efficiently compensated by the adsorption of electrolyte cations, thereby promoting the adsorption of phosphate (Tang et al. 2012; Yan et al. 2016).

The ^{31}P NMR spectra

To further explore the microscopic mechanisms for phosphate adsorption onto ZrMZ and HA-ZrMZ2, the solid-state ^{31}P NMR spectra of phosphate-adsorbed ZrMZ and phosphate-adsorbed HA-ZrMZ-2 were determined, and the results are shown in Fig. 10. The ^{31}P NMR spectrum for ZrMZ contained one major resonance signal centered at isotropic chemical shift = −6.802 ppm plus additional spinning sidebands (ssb). The ^{31}P NMR spectrum for HA-ZrMZ-2 contained one main resonance signal centered at isotropic chemical shift = −6.048 ppm plus additional ssb. Solid-state ^{31}P NMR spectroscopy is a good tool for identifying the chemical environment of phosphate adsorbed on metal oxides/hydroxides as well as for distinguishing inner-sphere complexes and outer-sphere complexes based on their chemical shifts (Li et al. 2013). Previous literatures have shown that the ^{31}P isotropic chemical shifts for solid alkaline phosphates and solution $H_xPO_4^{x-3}$ are in the range of 0–10 ppm (Kim and Kirkpatrick 2004; Mortlock et al. 1993). The outer-sphere phosphate surface complexes may have similar chemical environment to solid alkaline phosphates and solution $H_xPO_4^{x-3}$, and their isotropic chemical shifts may be between 0 and 10 ppm (Li et al. 2013). In the ^{31}P NMR spectrum,

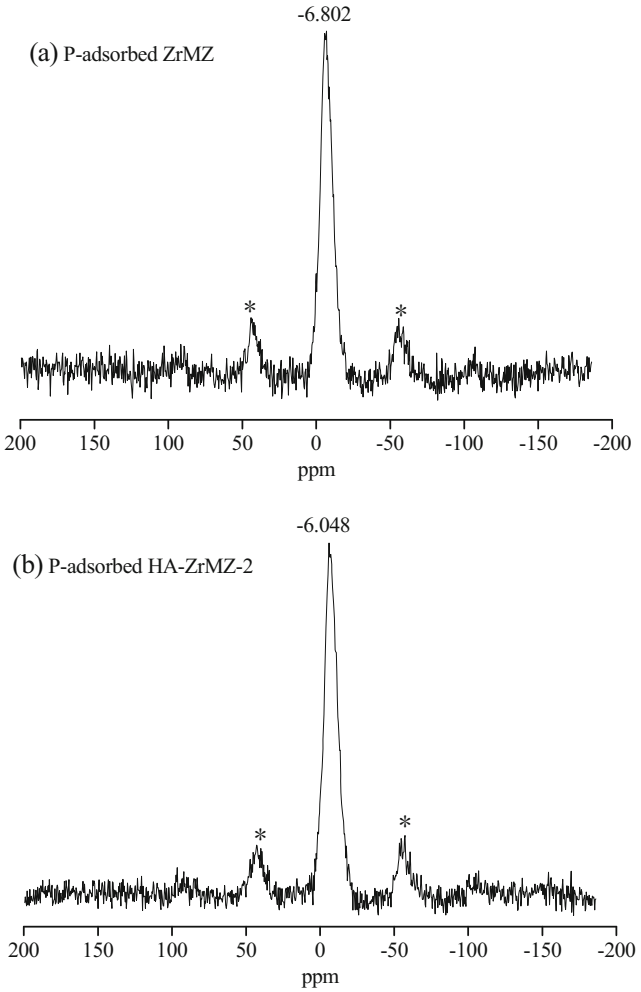

Fig. 10 The ^{31}P NMR spectra of **a** phosphate-adsorbed ZrMZ and **b** phosphate-adsorbed HA-ZrMZ-2

resonance signals in the range of $\delta_{P\text{-}31}$ = 0 to −6 ppm are typical for inner-sphere phosphate complexes on the aluminum (hydr)oxide surfaces (Li et al. 2013; Yan et al. 2015). Thus, the results obtained from Fig. 10 suggested that the adsorption of phosphate on ZrMZ and HA-ZrMZ at solution pH 7 mainly obeyed the inner-sphere complexing mechanism. For the ^{31}P NMR spectrum of zirconium phosphate, the resonance signals centered at −7, −14, and −21 were attributed to $(\equiv ZrO)PO(OH)_2$, $(\equiv ZrO)_2PO(OH)$, and $(\equiv ZrO)_3PO$, respectively (Zhang et al. 2010). In the ^{31}P NMR spectra of ZrMZ and HA-ZrMZ-2, the ^{31}P NMR signals assigned to the surface phosphate complexes were mainly located at 0 to −21 ppm, suggesting that the phosphate ions were mainly chemisorbed by one zirconium center and by bridging two zirconium centers to form monodentate surface complexes (e.g., $(\equiv ZrO)PO(OH)_2$ and $(\equiv ZrO)PO_2(OH)$) and bidentate binuclear surface complexes (e.g., $(\equiv ZrO)_2PO(OH)$), respectively, after the adsorption of phosphate on ZrMZ and HA-ZrMZ at solution pH 7.

Proposed mechanisms for phosphate adsorption onto ZrMZ and HA-ZrMZ

From all the experimental results that have been discussed above, it was suggested that the microscopic mechanism for phosphate adsorption onto ZrMZ and HA-ZrMZ at pH 7 was mainly the replacement of surface hydroxyl groups with phosphate anions and the formation of inner-sphere phosphate complexes at the solid/solution interface. This mechanism can be expressed as follows (Wang et al. 2016b; Zong et al. 2013):

$$\equiv Zr{-}OH + H_2PO_4^- = (\equiv Zr{-}O)PO_3H_2 + OH^- \quad (18)$$

$$\equiv Zr{-}OH + HPO_4^{2-} = (\equiv Zr{-}O)PO_3H^- + OH^- \quad (19)$$

$$2(\equiv Zr{-}OH) + HPO_4^{2-} = (\equiv Zr{-}O)_2PO_2H + 2OH^- \quad (20)$$

Effect of solution pH on phosphate adsorption

The effect of solution pH on phosphate adsorption onto ZrMZ, HA-ZrMZ-1, and HA-ZrMZ-2 is presented in Fig. 11. It was shown that the adsorption of phosphate on ZrMZ, HA-ZrMZ-1, and HA-ZrMZ-2 highly relied on solution pH. The phosphate adsorption capacities for ZrMZ, HA-ZrMZ-1, and HA-ZrMZ-2 decreased with increasing solution pH from 3 to 11 (Fig. 11), which is very similar to previous reports on phosphate adsorption onto other zirconium-containing adsorbents such as zirconia-functionalized graphite oxide (Zong et al. 2013), zirconia-functionalized SBA-15 (Tang et al. 2012), zirconium hydroxide (Johir et al. 2016), mesoporous ZrO_2 (Liu et al. 2008), zirconium(IV)-loaded, cross-linked chitosan particles (Liu et al. 2016a), and zirconia-loaded lignocellulosic butanol residue (Zong et al. 2016). Such a negative impact of pH increase on phosphate adsorption could be well explained by the electrostatic interaction between the phosphate anion and adsorbent as well as the ligand exchange mechanism. Under the investigated pH range (pH 3–11), phosphate existed in anionic forms (e.g., $H_2PO_4^-$ and HPO_4^{2-}), whereas the surface charge of ZrMZ, HA-ZrMZ-1, and HA-ZrMZ-2 changed with solution pH. The surface charges of ZrMZ, HA-ZrMZ-1, and HA-ZrMZ-2 were positive at solution pH below their pH_{PZC}, and in this case, the positively charged Zr-OH_2^+ and neutral Zr-OH groups prevailed on the adsorbent surface. An increase in solution pH from 3 to the pH_{PZC} of ZrMZ or HA-ZrMZ led to the decrease in the amount of the highly reactive, positively charge active adsorption sites (i.e., Zr–OH_2^+) (Wang et al. 2016b), thus giving rise of a decrease of phosphate adsorption capacity with increasing solution pH from 3 to the pH_{PZC} of ZrMZ or HA-ZrMZ. The ZrMZ, HA-ZrMZ-1, and HA-ZrMZ-2 were negatively charged at solution above their pH_{PZC}. The electrostatic repulsive interaction between the negatively charged adsorbent and phosphate anions could decrease the phosphate adsorption capacity, and this negative effect increased with the increase of solution pH from the pH_{PZC} of the adsorbent to 11. Furthermore, a rise in solution pH generally led in the increase of the amount of HPO_4^{2-} but the decrease of the amount of $H_2PO_4^-$. Since $H_2PO_4^-$ is favorable for ligand exchange because of its lower adsorption free energy, a decreasing adsorption took place with increasing solution pH (Wang et al. 2016b). Additionally, since OH^- ions could compete with phosphate ions for the adsorption active sites on the adsorbent surface, an increase in solution pH resulted in the increase of OH^- concentration, and this in turn led to a lower phosphate adsorption capacity at higher pH values (Wang et al. 2016a).

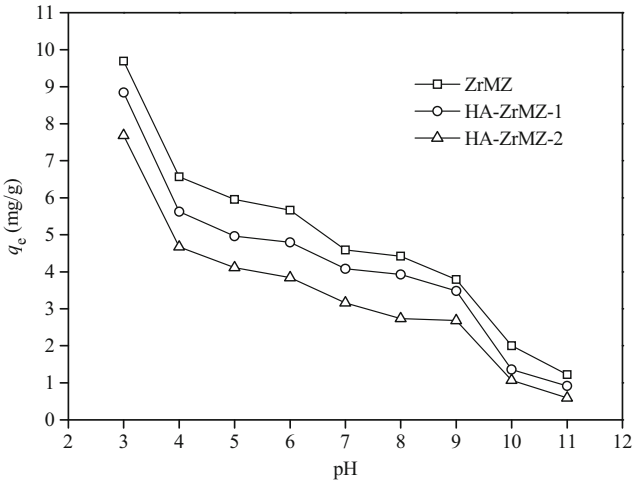

Fig. 11 Effect of solution pH on phosphate adsorption onto ZrMZ, HA-ZrMZ-1, and HA-ZrMZ-2

Figure 11 also shows that the amounts of phosphate adsorbed on HA-ZrMZ-1 and HA-ZrMZ2 at different pH values were higher than that of ZrMZ, suggesting that the preloading of HA on ZrMZ reduces the phosphate adsorption. Furthermore, the amounts of phosphate adsorbed on HA-ZrMZ-2 at different pH values were lower than that of HA-ZrMZ-1, suggesting a lower phosphate adsorption for HA-ZrMZ with a higher HA preloading amount.

Effect of coexisting cations and anions on phosphate adsorption

In natural water, there exist many cations and anions such as K^+, Na^+, Mg^{2+}, Ca^{2+}, Cl^-, HCO_3^-, SO_4^{2-}, and SiO_3^{2-} which might influence the adsorption of phosphate on ZrMZ, HA-ZrMZ-1, and HA-ZrMZ-2. In order to understand their effects, the effect of different electrolytes such as NaCl, Na_2SO_4, $NaHCO_3$, Na_2SiO_3, $CaCl_2$, $MgCl_2$, and KCl on the adsorption of phosphate on ZrMZ, HA-ZrMZ-1, and HA-ZrMZ-2 was investigated, and the results are presented in Fig. 12. It was shown that the presence of electrolytes such as NaCl, Na_2SO_4, $CaCl_2$, $MgCl_2$, and KCl enhanced the adsorption of phosphate on ZrMZ and HA-ZrMZ, and the positive effect was in the following order: $CaCl_2 > MgCl_2 > KCl > Na_2SO_4$ or NaCl. This indicated that

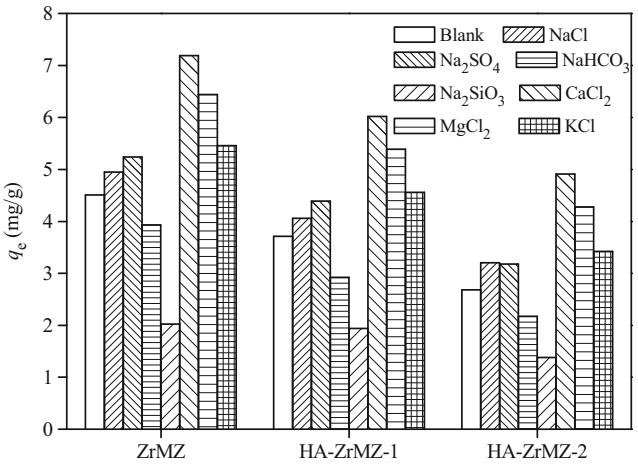

Fig. 12 Effect of coexisting electrolytes on phosphate adsorption onto ZrMZ, HA-ZrMZ-1, and HA-ZrMZ-2

coexisting anions such as Cl^- and SO_4^{2-} had no negative effect on the adsorption of phosphate on ZrMZ and HA-ZrMZ. Similar observations have been reported in previous literatures for the phosphate adsorption onto amorphous zirconium oxide nanoparticles (Su et al. 2013) and magnetite core/zirconia shell nanocomposite (Wang et al. 2016b). In contrast, coexisting cations such as Na^+, K^+, Mg^{2+}, and Ca^{2+} have a positive effect on the phosphate adsorption, and the positive effect was in the following order: $Ca^{2+} > Mg^{2+} > K^+ > Na^+$. The positive effect of cations such as Na^+, K^+, Mg^{2+}, and Ca^{2+} on the phosphate adsorption could be attributed to the neutralization of the negative surface charge on the phosphate inner-sphere complexes by the coadsorbed electrolyte cations (e.g., Na^+, K^+, Mg^{2+}, and Ca^{2+}) (Tang et al. 2012; Yan et al. 2016). The mechanism for the coadsorption of coexisting cations (e.g., K^+, Na^+, Ca^{2+}, and Mg^{2+}) and phosphate species (e.g., HPO_4^{2-}) on ZrMZ and HA-ZrMZ could be described by the following equations (Yan et al. 2016):

$$\equiv Zr{-}OH + HPO_4^{2-} + K^+ = (\equiv Zr{-}O)PO_3H^-K^+ + OH^- \quad (21)$$

$$\equiv Zr{-}OH + HPO_4^{2-} + Na^+ = (\equiv Zr{-}O)PO_3H^-Na^+ + OH^- \quad (22)$$

$$\equiv Zr{-}OH + HPO_4^{2-} + Ca^{2+} = (\equiv Zr{-}O)PO_3H^-Ca^{2+} + OH^- \quad (23)$$

$$\equiv Zr{-}OH + HPO_4^{2-} + Mg^{2+} = (\equiv Zr{-}O)PO_3H^-Mg^{2+} + OH^- \quad (24)$$

Figure 12 also shows that the presence of electrolytes such as $NaHCO_3$ and Na_2SiO_3 inhibited the adsorption of phosphate on ZrMZ and HA-ZrMZ, and the inhibited effect was in the following order: $Na_2SiO_3 > NaHCO_3$. Since coexisting Na^+ had a positive effect on the phosphate adsorption on ZrMZ and HA-ZrMZ, coexisting HCO_3^- or SiO_3^{2-} should had a negative effect on the phosphate adsorption. Furthermore, the negative effect of SiO_3^{2-} was much larger than that of HCO_3^-. A similar observation has been reported in a previous literature for the phosphate adsorption onto magnetite core/zirconia shell nanocomposite (Wang et al. 2016b). This phenomenon is probably due to the fact that the presence of HCO_3^- or SiO_3^{2-} competes with phosphate for the adsorption active sites on the adsorbent surfaces, thus lowering the phosphate adsorption capacity (Huang et al. 2015; Wang et al. 2016b).

Figure 12 also shows that the amounts of phosphate adsorbed on HA-ZrMZ in the presence of different electrolytes such as NaCl, Na_2SO_4, $NaHCO_3$, Na_2SiO_3, $CaCl_2$, $MgCl_2$, and KCl were lower than those of ZrMZ, indicating that the preloading of HA on ZrMZ inhibits the phosphate adsorption in the presence of cations (e.g., Na^+, K^+, Ca^{2+}, and Mg^{2+}) and anions (e.g., Cl^-, SO_4^{2-}, HCO_3^-, and SiO_3^{2-}). The amounts of phosphate adsorbed on HA-ZrMZ-2 in the presence of different electrolytes such as NaCl, Na_2SO_4, $NaHCO_3$, Na_2SiO_3, $CaCl_2$, $MgCl_2$, and KCl were lower than those of HA-ZrMZ-1, indicating that the HA-ZrMZ with a higher HA loading amount exhibits a lower phosphate adsorption capacity in the presence of cations (e.g., Na^+, K^+, Ca^{2+}, and Mg^{2+}) and anions (e.g., Cl^-, SO_4^{2-}, HCO_3^-, and SiO_3^{2-}).

Proposed mechanisms for effect of HA coating on phosphate adsorption

The preloading of HA on ZrMZ will influence the adsorption of phosphate in three ways. Firstly, since the ZrMZ surface had the same binding active sites for the adsorption of HA and phosphate, the preloading of HA on ZrMZ reduced the amount of binding active sites available for phosphate adsorption, resulting in the decreased phosphate adsorption capacity after the HA preloading. Secondly, the coating of HA would decrease the pH_{PZC} of ZrMZ, which would increase the amount of surface negative charge at pH higher the pH_{PZC} or decrease the amount of surface positive charge at pH lower than the pH_{PZC}. This would result in a reduction of the phosphate adsorption capacity due to the decrease of electrostatic attraction or due to the increase of electrostatic repulsion. Thirdly, the coating of HA would result in the decrease of the surface areas and pore volumes of ZrMZ. This indicated that the preloaded HA molecules not only could block the pores of adsorbents but also could cover some binding active sites available for phosphate adsorption, resulting in the decrease of the phosphate adsorption capacity after the HA coating.

Conclusion

Based on all the results discussed above, the main conclusions were drawn as follows: (1) the adsorption equilibrium data of phosphate on ZrMZ and HA-ZrMZ could be well described by the Langmuir, Freundlich, and D-R isotherm models; (2) the adsorption kinetic data of phosphate on ZrMZ and HA-ZrMZ well fitted with the pseudo-second-order kinetic model;

(3) the adsorption of phosphate on ZrMZ and HA-ZrMZ was a spontaneous and endothermic in nature; (4) the phosphate adsorption capacity for ZrMZ and HA-ZrMZ decreased with increasing pH from 3 to 11; (5) the adsorption of phosphate on ZrMZ and HA-ZrMZ could be inhibited by the presence of HCO_3^- and SiO_3^{2-}, but it could not be inhibited by the presence of Cl^- and SO_4^{2-}; (6) the presence of Na^+, K^+, Ca^{2+}, and Mg^{2+} enhanced the adsorption of phosphate on ZrMZ and HA-ZrMZ, and the positive effective was in the order of $Ca^{2+} > Mg^{2+} > K^+ > Na^+$; (7) the mechanisms for phosphate adsorption onto ZrMZ and HA-ZrMZ were mainly the formation of inner-sphere phosphate complexes at the solid/solution interface; (8) the preloading of HA on ZrMZ reduced the adsorption of phosphate, and the more the HA loading amount is, the lower the phosphate adsorption capacity is; and (9) the decreased phosphate adsorption capacity for ZrMZ could be due to the fact that the coating of HA on ZrMZ reduced the amount of binding active sites available for phosphate adsorption, changed the adsorbent surface charges, and reduced the specific surface areas and pore volumes of ZrMZ.

Acknowledgments This research was supported by the National Natural Science Foundation of China (51408354, 50908142), the Shanghai Natural Science Foundation (15ZR1420700), and the Scientific Research Project of Shanghai Science and Technology Committee (10230502900).

References

Berg U, Neumann T, Donnert D, Nüesch R, Stüben D (2004) Sediment capping in eutrophic lakes-efficiency of undisturbed calcite barriers to immobilize phosphorus. Appl Geochem 19:1759–1771

Chekli L, Phuntsho S, Roy M, Shon HK (2013) Characterisation of Fe-oxide nanoparticles coated with humic acid and Suwannee River natural organic matter. Sci Total Environ 461–462:19–27

Chen B, Zhu ZL, Guo YW, Qiu YL, Zhao JF (2013) Facile synthesis of mesoporous Ce–Fe bimetal oxide and its enhanced adsorption of arsenate from aqueous solutions. J Colloid Interface Sci 398:142–151

Chen QQ, Yin DQ, Zhu SJ, Hu XL (2012) Adsorption of cadmium(II) on humic acid coated titanium dioxide. J Colloid Interface Sci 367: 241–248

Chitrakar R, Tezuka S, Sonoda A, Sakane K, Ooi K, Hirotsu T (2006) Selective adsorption of phosphate from seawater and wastewater by amorphous zirconium hydroxide. J Colloid Interface Sci 297:426–433

Correll DL (1998) The role of phosphorus in the eutrophication of receiving water: a review. J Environ Qual 27:261–266

Cui H, Li Q, Gao S, Shang JK (2012) Strong adsorption of arsenic species by amorphous zirconium oxide nanoparticles. J Ind Eng Chem 18: 1418–1427

D'Arcy M, Weiss D, Bluck M, Vilar R (2011) Adsorption kinetics, capacity and mechanism of arsenate and phosphate on a bifunctional TiO_2–Fe_2O_3 bi-composite. J Colloid Interface Sci 364:205–212

Dai LC, Pan G (2014) The effects of red soil in removing phosphorus from water column and reducing phosphorus release from sediment in Lake Taihu. Water Sci Technol 69:1052–1058

Erhayem M, Sohn M (2014) Effect of humic acid source on humic acid adsorption onto titanium dioxide nanoparticles. Sci Total Environ 470–471:92–98

Freundlich H (1926) Colloid and capillary chemistry. Methuen, London

Funes A, de Vicente J, Cruz-Pizarro L, Álvarez-Manzaneda I, de Vicente I (2016) Magnetic microparticles as a new tool for lake restoration: a microcosm experiment for evaluating the impact on phosphorus fluxes and sedimentary phosphorus pools. Water Res 89:366–374

Gheju M, Balcu I, Mosoarca G (2016) Removal of Cr(VI) from aqueous solutions by adsorption on MnO_2. J Hazard Mater 310:270–277

Gibbs M, Özkundakci D (2011) Effects of a modified zeolite on P and N processes and fluxes across the lake sediment–water interface using core incubations. Hydrobiologia 661:21–35

Guaya D, Valderrama C, Farran A, Armijos C, Cortina JL (2015) Simultaneous phosphate and ammonium removal from aqueous solution by a hydrated aluminum oxide modified natural zeolite. Chem Eng J 271:204–213

Ho YS, McKay G (1999) Pseudo-second order model for sorption processes. Process Biochem 34:451–465

Huang WY, Chen J, He F, Tang JP, Li D, Zhu Y, Zhang YM (2015) Effective phosphate adsorption by Zr/Al-pillared montmorillonite: insight into equilibrium, kinetics and thermodynamics. Appl Clay Sci 104:252–260

Ichihara M, Nishio T (2013) Suppression of phosphorus release from sediments using water clarifier sludge as capping material. Environ Technol 34:2291–2299

Islam M, Mishra PC, Patel R (2013) Microwave assisted synthesis of polycinnamamide Mg/Al mixed oxide nanocomposite and its application towards the removal of arsenate from aqueous medium. Chem Eng J 230:48–58

Jeppesen E, Sondergaard M, Jensen JP, Havens KE, Anneville O, Carvalho L, Coveney MF, Deneke R, Dokulil MT, Foy B, Gerdeaux D, Hampton SE, Hilt S, Kangur K, Kohler J, Lammens E, Lauridsen TL, Manca M, Miracle MR, Moss B, Noges P, Persson G, Phillips G, Portielje R, Schelske CL, Straile D, Tatrai I, Willen E, Winder M (2005) Lake responses to reduced nutrient loading-an analysis of contemporary long-term data from 35 case studies. Freshw Biol 50:1747–1771

Johir MAH, Pradhan M, Loganathan P, Kandasamy J, Vigneswaran S (2016) Phosphate adsorption from wastewater using zirconium (IV) hydroxide: kinetics, thermodynamics and membrane filtration adsorption hybrid system studies. J Environ Manag 167:167–174

Kim Y, Kirkpatrick RJ (2004) An investigation of phosphate adsorbed on aluminium oxyhydroxide and oxide phases by nuclear magnetic resonance. Eur J Soil Sci 55:243–251

Kumar S, Rawat N, Kar AS, Tomar BS, Manchanda VK (2011) Effect of humic acid on sorption of technetium by alumina. J Hazard Mater 192:1040–1045

Lürling M, Waajen G, van Oosterhout F (2014) Humic substances interfere with phosphate removal by lanthanum modified clay in controlling eutrophication. Water Res 54:78–88

Langmuir I (1916) The constitution and fundamental properties of solids and liquids part I. Solid J Am Chem Soc 38:2221–2295

Li W, Pierre-Louis A-M, Kwon KD, Kubicki JD, Strongin DR, Phillips BL (2013) Molecular level investigations of phosphate sorption on corundum (α-Al_2O_3) by ^{31}P solid state NMR, ATR-FTIR and quantum chemical calculation. Geochim Cosmochim Ac 107:252–266

Liang L, Lv JT, Luo L, Zhang J, Zhang SZ (2011) Influences of surface-coated fulvic and humic acids on the adsorption of metal cations to SiO_2 nanoparticles. Colloid Surface A 389:27–32

Lin JW, Zhan YH, Zhu ZL (2011a) Adsorption characteristics of copper (II) ions from aqueous solution onto humic acid-immobilized surfactant-modified zeolite. Colloid Surface A 384:9–16

Lin JW, Zhan YH, Zhu ZL (2011b) Evaluation of sediment capping with active barrier systems (ABS) using calcite/zeolite mixtures to simultaneously manage phosphorus and ammonium release. Sci Total Environ 409:638–646

Liu HL, Sun XF, Yin CQ, Hu C (2008) Removal of phosphate by mesoporous ZrO_2. J Hazard Mater 151:616–622

Liu J, Su Y, Li Q, Yue QY, Gao BY (2013) Preparation of wheat straw based superabsorbent resins and their applications as adsorbents for ammonium and phosphate removal. Bioresour Technol 143:32–39

Liu Q, Hu P, Wang J, Zhang LJ, Huang RH (2016a) Phosphate adsorption from aqueous solutions by zirconium (IV) loaded cross-linked chitosan particles. J Taiwan Inst Chem E 59:311–319

Liu S, Lim M, Amal R (2014) TiO_2-coated natural zeolite: rapid humic acid adsorption and effective photocatalytic regeneration. Chem Eng Sci 105:46–52

Liu SJ, Li J, Yang YK, Wang J, Ding H (2016b) Influence of environmental factors on the phosphorus adsorption of lanthanum-modified bentonite in eutrophic water and sediment. Environ Sci Pollut Res 23:2487–2494

Lu JB, Liu DF, Hao J, Zhang GW, Lu B (2015) Phosphate removal from aqueous solutions by a nano-structured Fe–Ti bimetal oxide sorbent. Chem Eng Res Des 93:652–661

Mortlock RF, Bell AT, Radke CJ (1993) ^{31}P and ^{27}Al NMR investigations of the effects of pH on aqueous solutions containing aluminum and phosphorus. J Phys Chem 97:775–782

Pan XL, Wang JL, Zhang DY (2009) Sorption of cobalt to bone char: kinetics, competitive sorption and mechanism. Desalination 249: 609–614

Reitzel K, Andersen FØ, Egemose S, Jensen HS (2013) Phosphate adsorption by lanthanum modified bentonite clay in fresh and brackish water. Water Res 47:2787–2796

Reitzel K, Hansen J, Jensen HS, Andersen FØ, Hansen KS (2003) Testing aluminum addition as a tool for lake restoration in shallow, eutrophic lake Sønderby, Denmark. Hydrobiologia 506:781–787

Rodrigues LA, Maschio LJ, Coppio Lde S, Thim GP, da Silva ML (2012) Adsorption of phosphate from aqueous solution by hydrous zirconium oxide. Environ Technol 33:1345–1351

Søndergaard M, Jensen J, Jeppesen E (2003) Role of sediment and internal loading of phosphorus in shallow lakes. Hydrobiologia 506-509: 135–145

Seliem MK, Komarneni S, Abu Khadra MR (2016) Phosphate removal from solution by composite of MCM-41 silica with rice husk: kinetic and equilibrium studies. Micropor Mesopor Mater 224:51–57

Smith VH, Tilman GD, Nekola JC (1999) Eutrophication: impacts of excess nutrient inputs on freshwater, marine, and terrestrial ecosystems. Environ Pollut 100:179–196

Song YC, Subha B, Woo JH, Lim HJ, Senthilkumar P (2014) Surface modification of sediment with surfactant for capping material on contaminated coastal sediment. Water Air Soil Poll 225:2067–2076

Stern JC, Foustoukos DI, Sonke JE, Salters VJM (2014) Humic acid complexation of Th, Hf and Zr in ligand competition experiments: metal loading and pH effects. Chem Geol 363:241–249

Su Y, Cui H, Li Q, Gao SA, Shang JK (2013) Strong adsorption of phosphate by amorphous zirconium oxide nanoparticles. Water Res 47:5018–5026

Su Y, Yang WY, Sun WZ, Li Q, Shang JK (2015) Synthesis of mesoporous cerium–zirconium binary oxide nanoadsorbents by a solvothermal process and their effective adsorption of phosphate from water. Chem Eng J 268:270–279

Sun DD, Lee PF (2012) TiO_2 microsphere for the removal of humic acid from water: complex surface adsorption mechanisms. Sep Purif Technol 91:30–37

Tang YQ, Zong EM, Wan HQ, Xu ZY, Zheng SR, Zhu DQ (2012) Zirconia functionalized SBA-15 as effective adsorbent for phosphate removal. Micropor Mesopor Mater 155:192–200

Wang CH, Pei YS (2013) A comparison of the phosphorus immobilization capabilities of water treatment residuals before and after settling from lake water. Sep Purif Technol 117:83–88

Wang CH, Yuan NN, Pei YS, Jiang HL (2015a) Aging of aluminum/iron-based drinking water treatment residuals in lake water and their association with phosphorus immobilization capability. J Environ Manag 159:178–185

Wang H, Zhu J, Fu QL, Xiong JW, Hong C, Hu HQ, Violante A (2015b) Adsorption of phosphate onto ferrihydrite and ferrihydrite-humic acid complexes. Pedosphere 25:405–414

Wang Z, Lin Y, Wu DY, Kong HN (2016a) Hydrous iron oxide modified diatomite as an active filtration medium for phosphate capture. Chemosphere 144:1290–1298

Wang Z, Xing MC, Fang WK, Wu DY (2016b) One-step synthesis of magnetite core/zirconia shell nanocomposite for high efficiency removal of phosphate from water. Appl Surf Sci 366:67–77

Weber WJ, Morris JC (1964) Equilibria and capacities for adsorption on carbon. J Sanit Eng Div 90:79–107

Yamamoto T, Harada K, Kim KH, Asaoka S, Yoshioka I (2013) Suppression of phosphate release from coastal sediments using granulated coal ash. Estuar Coast Shelf Sci 116:41–49

Yan JL, Jiang T, Yao Y, Lu S, Wang QL, Wei SQ (2016) Preliminary investigation of phosphorus adsorption onto two types of iron oxide-organic matter complexes. J Environ Sci 42:152–162

Yan YP, Koopal LK, Li W, Zheng AM, Yang J, Liu F, Feng XH (2015) Size-dependent sorption of myo-inositol hexakisphosphate and orthophosphate on nano-γ-Al_2O_3. J Colloid Interface Sci 451:85–92

Yang MJ, Lin JW, Zhan YH, Zhang HH (2014) Adsorption of phosphate from water on lake sediments amended with zirconium-modified zeolites in batch mode. Ecol Eng 71:223–233

Yang MJ, Lin JW, Zhan YH, Zhu ZL, Zhang HH (2015) Immobilization of phosphorus from water and sediment using zirconium-modified zeolites. Environ Sci Pollut R 22:3606–3619

Yin HB, Kong M, Fan CX (2013) Batch investigations on P immobilization from wastewaters and sediment using natural calcium rich sepiolite as a reactive material. Water Res 47:4247–4258

Zhang JN, Ma Z, Jiao J, Yin HF, Yan WF, Hagaman EW, Yu JH, Dai S (2010) Surface functionalization of mesoporous silica SBA-15 by liquid-phase grafting of zirconium phosphate. Micropor Mesopor Mater 129:200–209

Zhang WQ, Shan BQ, Li J, Tang WZ, Jin X, Zhang H, Ding YK, Wang YY, Zhu XL (2015) Characteristics, distribution and ecological risk assessment of phosphorus in surface sediments from different ecosystems in eastern China: a ^{31}P-nuclear magnetic resonance study. Ecol Eng 75:264–271

Zhang WQ, Shi L, Tang KB, Liu ZP (2012) Synthesis, surface group modification of 3D MnV_2O_6 nanostructures and adsorption effect on rhodamine B. Mater Res Bullet 47:1725–1733

Zhou YL, Zhang YB, Li GH, Wu YD, Jiang T (2015) A further study on adsorption interaction of humic acid on natural magnetite, hematite and quartz in iron ore pelletizing process: effect of the solution pH value. Powder Technol 271:155–166

Zhou YL, Zhang YB, Li P, Li GH, Jiang T (2014) Comparative study on the adsorption interactions of humic acid onto natural magnetite, hematite and quartz: effect of initial HA concentration. Powder Technol 251:1–8

Zhu MY, Zhu GW, Li W, Zhang YL, Zhao LL, Gu Z (2013) Estimation of the algal-available phosphorus pool in sediments of a large, shallow eutrophic lake (Taihu, China) using profiled SMT fractional analysis. Environ Pollut 173:216–223

Zong E, Liu X, Jiang J, Fu S, Chu F (2016) Preparation and characterization of zirconia-loaded lignocellulosic butanol residue as a biosorbent for phosphate removal from aqueous solution. Appl Surf Sci 387:419–430

Zong EM, Wei D, Wan HQ, Zheng SR, Xu ZY, Zhu DQ (2013) Adsorptive removal of phosphate ions from aqueous solution using zirconia-functionalized graphite oxide. Chem Eng J 221:193–203